ISSN 1330-3651 (Print), ISSN 1848-6339 (Online)
https://doi.org/10.17559/TV-20220407215830
Original scientific paper

Influence of Purging Gas on 316L Stainless Steel Fusion Zone in Autogenous Stationary TIG Welding

Domagoj KOJUNDŽIĆ*, Nikša KRNIĆ, Ivan SAMARDŽIĆ, Pejo KONJATIĆ

Abstract: This research reveals the influence of different purging conditions on the fusion zone dimensions and shape for stationary autogenous TIG welding of 316L stainless steel. Welding experiments were performed for unpurged and purged weld root side for 7, 14 and 21 second arcing time. Purging was executed with ten seconds of pre-flow and 23 seconds of post-flow with 10 l/min Ar and 4 l/min of He. Characteristic fusion zone dimensions were extracted and calculated from photo-macrographs of weld cross-sections. Purging the weld root side by argon increased penetration depth and cross-section area compared to helium. Those benefits of argon purging can be attributed to its low thermal conductivity. Measurement of thermal cycles on the weld root side revealed that peak temperatures were higher by argon purging compared to the presence of helium or air. The fusion zone width exhibited no significant differences regardless of weld root side gas type.

Keywords: argon; autogenous TIG; fusion zone; helium; penetration; purging gas, stainless steel 316L; stationary TIG welding

1 INTRODUCTION

The austenitic stainless steels (ASS) belong to the subgroup of the broad stainless steel (SS) family. These iron-based alloys contain adequate amounts of chromium and nickel and have austenitic crystal structure in a wide temperature range. They were developed at the beginning of the 20th century in the Krupp Laboratories in Germany. Shortly later, 18-8 CrNi stainless steels have been introduced. Austenitic stainless steels are in broad use nowadays, especially in the food, chemical, transportation and oil industries. They are well-known for their corrosion and oxidation resistance, good formability and weldability, [1, 2].

Some physical properties of ASS are significantly different compared to carbon steels. Their thermal conductivity is approximately 30% that of the mild steel, while the melting point is about 100 °C lower. The electrical resistance of ASS is approximately 8 times that of mild steel and the coefficient of ASS thermal expansion is about 50% greater compared to mild steel.

Research activity on ASS welding has been covering all aspects of weldability and welding process applications. Almost all main welding processes have been applied for ASS welding. In both scientific and industrial areas, the most frequently used process is electric arc welding with non-consumable tungsten electrode and inert shielding gas. This process is usually abbreviated as TIG (Tungsten Inert Gas) or GTA (Gas Tungsten Arc) welding. TIG welding process produces high quality welded joints but suffers from relatively low productivity and small weld penetration, [3]. The low penetration profile of TIG weldments in ASS is characterised by a rather shallow and wide fusion zone. The formation and evolution of the fusion zone during welding is a complex process governed by heat transfer from the electric arc to the workpiece. Several different, simultaneously acting forces govern the formation and behaviour of the weld pool and affect the final fusion zone shape. These forces, as well as the amount of heat generated in the electric arc, are controlled by the welding parameters, [4-6]. Because of complex formation, weld fusion zone often has been a research subject. The usual way of fusion zone shape characterisation is obtained by dividing weld penetration depth (D) and weld width (W). This depth-to-width or D/W ratio is also called the fusion zone aspect ratio.

Weld morphology, weld pool geometry, weld bead profile or fusion zone shape formed under autogenous TIG welding of ASS (304, 316, 316L, 4 mm, 5 mm and 6 mm thick) were investigated and correlated with welding parameters such as current intensity, welding speed, arc length, electrode vertex angle, workpiece position, shielding gas chemical composition and activating elements, [7-12]. It is well known that very small amounts of surface-active elements (S, O, Se) in stainless steel can significantly influence the weld shape and dimensions under the same welding parameters, [4, 13, 14]. These surface-active elements affect the liquid metal surface tension and its temperature dependency. Surface tension is an important factor because it can cause two fundamentally different circular molten metal flows in the weld pool thus affecting fusion zone dimensions, [5].

Optimisation of welding parameters in autogenous pulsed TIG welding process on 3 mm thick 304L stainless steel (root side purging Ar 5 l/min) to obtain weld bead area and aspect ratio was performed in [15]. Optimisation of pulsed orbital TIG welding on 3mm thick 316L pipe was studied in [16].

Various surface-active fluxes significantly increase penetration and corresponding fusion zone D/W ratio for ASS TIG welding, [17, 18]. It was also demonstrated that high-frequency pulsed TIG welding increases arc stiffness and energy density which can improve weld penetration depth, [19]. The TIG process variant called K-TIG (Keyhole-TIG) was developed specifically to overcome shallow penetration and low productivity associated with the conventional TIG process [20].

Less investigation interest has been associated with stationary or spot TIG welding configuration compared to moving TIG. Weld pool dimensions and shape for stationary TIG process on 50 mm cylinder shaped 10 mm thick 304L ASS backed by copper disc were studied for welding time from 1 s to 20 s, [21]. Effects of arc current intensity, electrode to BM distance, vertex angle and two shielding gases (He and He + 30Ar) on the evolution of the fusion zone were mainly explained by temperature changes in base metal thermal diffusivity. Increased welding

current and arc length increased weld width and depth. Helium resulted in a deeper weld pool compared to the Ar He mixture. Electrode vertex angle was not a significant factor but when decreased it increased penetration slightly. It was found that hydrogen in argon shielding gas increased the arc efficiency.

Effects of typical purging gases on the microstructural, corrosion and mechanical properties of stainless steel were studied too, [22-24]. Purging or backing gas assure high-quality root of stainless steel welds. They prevent the formation of undesirable thick oxides which decrease mechanical properties and corrosion resistance of the joint. Common gases used for the weld root side shielding are argon, helium, nitrogen and their mixtures with hydrogen.

However, there is no available data on the influence of weld root side purging gas type on fusion zone shape and dimensions for stationary TIG welding. This work investigates how the presence of helium, argon or air on the weld root side affects the resulting fusion zone shape and dimensions. The paper also gives a better insight into the TIG welding process repeatability (variations in fusion zone dimensions) under the same welding parameters.

Experiments were performed on 316L austenitic stainless steel by stationary TIG welding process for welding time of 7 s, 14 s and 21 seconds.

2 EXPERIMENTAL WORK AND METHODOLOGY

2.1 Experimental Setup

The experimental setup enabled stationary autogenous (without filler metal) TIG welding for the desired time on the selected base metal. The TIG power source was governed by the external, self-developed system with a PL microcontroller. The control loop could be programmed to select desired time of electric arc action in a tenth of a second (1/10 s). A light signal from an electric arc was captured by an optical cable at the very beginning of arc activation and transmitted to the light-dependent (LDR) sensor that was connected to the PL microcontroller. The timer counted down the welding time and switched off the welding current when desired welding time was reached. The main system components for welding experiments were a TIG power source (INVERTER ACCUTIG AVP-300P) with a welding gun along with two fixtures and a system for purging gas application. The welding power source enables the application of AC, DC or pulsed welding current up to the intensity of 300 A. Gas-cooled welding gun was equipped with a collar for a 2,4 mm electrode.

A thoriated tungsten electrode 2,4 mm in diameter with a conical sharp tip (no truncation) and vertex angle of 45° was used. The electrode tip was longitudinally sharpened by grinding according to the established practice on a dedicated electrode grinder.

One fixture was used to position and hold the welding gun at the fixed position during the application of the welding arc on the base metal. It had three axes of freedom necessary to position the welding gun in a suitable space point (centre of the surface plane and the desired distance from electrode tip to the workpiece). The other fixture was a four-point clamping device for sample accommodation. The fixture had to minimise cooling losses from the treated specimen by heat conduction and enable symmetric current flow through base metal. Owing to the clamping method, cooling of the specimen during and after the application of TIG electric arc was governed primarily by natural convection and radiation heat transfer.

The system for application of the purging gas was designed to ensure a uniform gas supply on the specimen's root side. It was manufactured from a square (45 mm × 45 mm) steel tube with a perforated insert plate (grid of fine bores). The appliance was positioned 1 mm from the bottom side of the specimen and centred.

Following schematic representation gives insight into welding clamping methodology, Fig. 1.

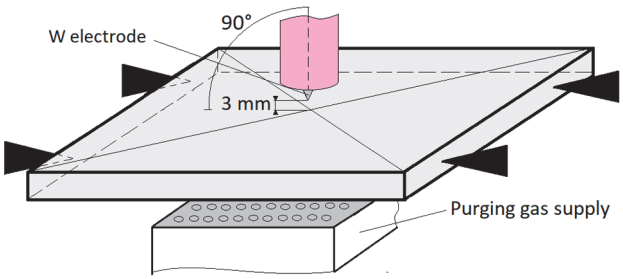

Figure 1 Specimen clamping and position of the heat application of the TIG electric arc (location is equidistant from edge boundaries of the specimen)

2.2 Base Metal Alloy and Purging Gases

The research was performed on square-shaped, 100 mm × 100 mm, base metal 5 mm thick. The base metal specimens were cut from austenitic stainless steel AISI 316L (EN 1.4404 X2CrNiMo17-12-2). It is high alloyed stainless steel intended for welding (low percentage of carbon) and structural applications that has good pitting corrosion resistivity. According to the fabricator's certificate, steel obtained 1D (No. 1 acc. to ASTM) mill finish after hot rolling, annealing (at 1050 °C) and scale removing (pickling). The chemical composition of 316L stainless steel is shown in Tab. 1. Solidus and liquidus temperatures for 316L ASS are 1402 °C and 1435 °C respectively, [25].

Table 1 The chemical composition of 316L stainless steel

El.	C	Si	Mn	P	S	Cr	Ni	Mo	N
wt. / %	0,023	0,571	1,36	0,0289	0,0111	17,067	10,558	2,14	0,0556

Purging of the weld root side prevents the formation of thicker surface oxides on ASS thus diminishing the potential pitting and intergranular corrosion issues. Not all of the gases exhibit the same surface protecting efficacy and that is why different purging gases were evaluated in this work.

Argon with 4.8 purity was used as shielding gas in all experiments and as a purging gas in some of them. Helium 5.0 purity was also applied as a purging gas in some of the experiments. Helium and argon have significantly different thermal and general physical properties. For example, relative densities of He and Ar are 0,14 and 1,38 compared to air. The thermal conductivities of three gases whose effects on the weld fusion zone were investigated are shown in Fig. 2.

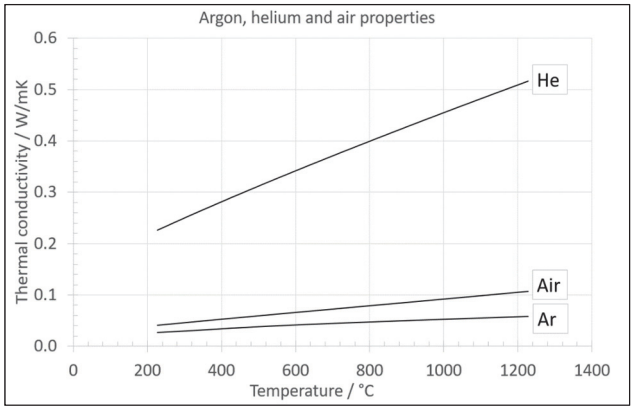

Figure 2 Thermal conductivities of He and Ar used in experimentation as purging gas compared to air, according to the data from [26]

2.3 Experimental Plan for Effects of Purging gases

The main goal of this research was to investigate the effects of root side purging gas and specimen surface preparation on the fusion zone geometry by stationary autogenous TIG welding arc on the 5 mm thick 316L stainless steel. Every welding experiment was repeated under strictly identical welding conditions. Measured characteristic fusion zone dimensions enabled calculations of averaged values and assured insight into process repeatability. The set of three experimental repetitions for every observed welding time was performed. Before the main investigation, suitable surface roughness was established by preliminary testing. Obtaining the uniform surface roughness and eliminating the surface mill variations was performed by light hand grinding (very low pressure) of the specimen surfaces. They were ground with SiC sandpaper (P#120 followed by P#400 and finally P#800 grain size). On the root side, initial grinding was performed by electrically driven hand grinding machine followed by the above-mentioned hand procedure. The specimen surface roughness was measured using the portable surface roughness tester SJ301.

Table 2 Experiments for investigation of purging gas type effects on a fusion zone in stationary autogenous TIG welding on 5 mm thick 316L stainless steel

Gas type gas flow rate / l/min (root side)	Face or root side roughness *Ra* / µm	Arc acting time/ s	Experiment
Argon (purging) / 10	1,81/1,14	7	Ar71
			Ar72
			Ar73
		14	Ar141
			Ar142
			Ar143
		21	Ar211
			Ar212
			Ar213
Helium (purging) / 4		7	He71
			He72
			He73
		14	He141
			He142
			He143
		21	He211
			He212
			He213

Tab. 2 represents the experiments that were planned to reveal the effects of root side purging gas type on 316L steel TIG fusion zone. The main criteria for purging gas flow rate selection were the quality of root side protection against oxidation and the comparability of obtained results between helium and argon. Additionally, the idea was to minimise the gas flow rate for both gases (argon and helium) due to environmental protection and cost reduction. Suitable gas flow rates were chosen after a series of preliminary experiments for the longest welding time of 21 seconds. Finally, the gas flow rates of 10 l/min for argon and 4 l/min for helium were used in all experiments for root side purging. Purging was activated 10 s before arc start and was active during arcing followed by 23 seconds of post flow.

Unpurged or unprotected weld root side served as a control group of experiments in which stagnant air was in contact with the original, previously hot rolled 316L stainless steel surface, Tab. 3.

Table 3 Experiments for the control results of unprotected weld root side in stationary autogenous TIG welding on 5 mm thick 316L stainless steel

Unpurged (unprotected) weld root side Gas type and flow rate / l/min(root side)	Face or root side mean roughness *Ra* / µm	Arc acting time / s	Experiment
Air (stagnant) / 0	1,81/1,14	7	Air71
			Air72
			Air73
		14	Air141
			Air142
			Air143
		21	Air211
			Air212
			Air213

Table 4 Welding parameters applied in stationary autogenous TIG welding on 5 mm thick 316L stainless steel

Welding parameter	Type/value
Current type	Direct current (DC)
Electrode polarity	Electrode negative (EN, SP)
Current intensity	150 A
W electrode diameter	2,4 mm
W electrode type	2 % Th (red labelled)
Vertex angle of the W electrode	45°
Truncation of the W electrode	0 mm
W electrode stick-out	3 mm
Gap from W electrode tip to BM	3 mm
Electrode to workpiece angle	90°
Shielding gas	Argon 4.8
Shielding gas flow rate	8 l/min
Shielding gas nozzle diameter	Ø 11 mm (size 7)
Welding position	PA (downhand, flat)

Before every welding experiment specimen surfaces were thoroughly degreased using denatured alcohol. Special attention has been devoted to obtaining the perfect horizontal specimen position because even small inaccuracies can result in unsymmetrical penetration profiles.

The same welding parameters, summarised in Tab. 4, were used in all welding experiments.

This procedure was conducted in order to isolate the separation line between fused weld metal and the solid-state part of the specimen and to evaluate the fusion zone shape and dimensions. Specimens were cut on a water-cooled sectioning machine along the diameter line enabling insight into the true cross-section of welded specimen. Each specimen was ground in three steps finalising with waterproof silicon carbide paper with grain size P#180 (micro grit acc. to standards of abrasive producers FEPA).

Macrostructure was revealed after approximately 15 minutes of immersion etching in an aqueous mixture of hydrofluoric and hydrochloric acid (5:4:2parts of H_2O:HF:HCl). Photos of macrostructures for weld fusion zone characterisation were taken on a stereo zoom optical microscope under suitable magnifications.

Finally, fusion zone geometry and area were analysed using open-source image processing software Image J. The quantitative metrics used to evaluate fusion zone shape and dimensions were fusion zone width, depth and cross-section area, Fig. 3. If maximum fusion zone depth is not positioned in the specimen centre, the value is obtained by averaging the centre and both lateral penetrations. The fusion zone depth-to-width ratio (D/W ratio) was also calculated. Measuring errors due to the resolution and fusion line uncertainty issues (mushy zone, lighting conditions, etching outcome) were in the range of approximately ±2%.

Temperature measurements were performed by digital thermometer and K-type thermocouples (TC) of 0,5 mm diameter wires. For every measurement new TC tip was formed by gas welding, the typical hot junction diameter was about 1 mm.

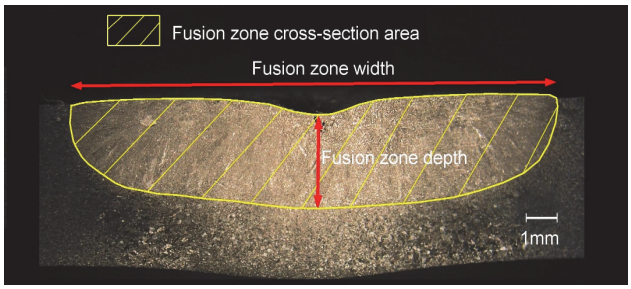

Figure 3 Fusion zone characteristic elements-width, penetration depth and cross-section area

The temperature sampling rate was 1 Hz. Welding thermal cycles were constructed from sampled data. Thermocouples were welded to the root side of the specimen by percussion welding using proprietary, self-made capacitor welding apparatus. Every TC was welded in the centre of the specimen's root side (intersection of two diagonals) directly underneath the axis of the electric arc. Welding of TC on the root side was performed by hand and the realised position of the thermocouple was not ideal every time. To consider the influence of the measurement position on the peak temperature the distance from the actual position to the centre of the arc acting point was measured (r_e value in Tab. 5).

3 RESULTS

The summary of measured fusion zone (FZ) width, depth and cross-section area for different types of gases on the weld root side (argon, helium, air) and different welding time (7, 14 and 21 seconds) is shown in Tab. 6.

Tab. 7 gives insight into characteristic values of weld fusion zones for unprotected or unpurged weld root sides.

The measured thermal cycles for argon, helium and air on the weld root side and welding times of 7, 14 and 21 seconds are shown in Fig. 4.

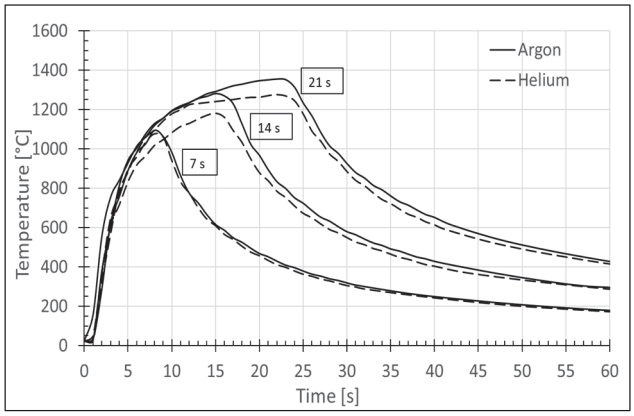

Figure 4 Thermal cycles for welding time of 7, 14 and 21 seconds with argon and helium and air on the weld root side

The peak temperatures (T_{max}) measured for different welding times in the middle of the specimen's root side and thermocouple position errors (r_e) are shown in Tab. 5.

Table 5 Measured peak temperatures and distance of thermocouple to the ideal centre

	Time of arc action					
	7 s		14 s		21 s	
Purging gas	Ar	He	Ar	He	Ar	He
T_{max} / °C	1095	1076	1280	1181	1354	1277
r_e / mm	0,72	1,20	0,3	1,12	2,06	0,5

Table 6 Characteristic weld fusion zone (FZ) values obtained according to the experimentation plan from **Tab. 2**

Fusion zone (FZ)											
Exp.	Width / mm	Depth / mm	Area / mm^2	Exp.	Width / mm	Depth / mm	Area / mm^2	Exp.	Width / mm	Depth / mm	Area / mm^2
Ar71	11,70	1,59	16,10	Ar141	13,75	3,59	43,00	Ar211	15,43	4,22	54,36
Ar72	11,85	1,42	14,70	Ar142	13,90	2,89	35,35	Ar212	16,20	3,55	45,68
Ar73	11,80	1,38	15,21	Ar143	14,05	2,50	34,83	Ar213	15,70	3,93	52,20
He71	11,80	1,48	15,80	He141	13,90	2,50	32,84	He211	15,90	3,35	43,82
He72	11,50	1,45	15,51	He142	13,80	2,78	36,20	He212	15,85	3,42	46,54
He73	11,55	1,42	15,40	He143	13,80	2,46	31,10	He213	16,25	2,88	40,83

Table 7 Characteristic fusion zone (FZ) values obtained according to the experimentation plan from **Tab. 3**

Fusion zone (FZ)											
Exp.	Width / mm	Depth / mm	Area / mm^2	Exp.	Width / mm	Depth / mm	Area / mm^2	Exp.	Width / mm	Depth / mm	Area / mm^2
Air71	12,20	1,40	15,37	Air141	13,85	2,73	34,97	Air211	15,70	3,46	47,50
Air72	11,95	1,42	15,22	Air142	14,55	2,33	31,46	Air212	15,95	3,35	46,95
Air73	11,50	1,42	14,83	Air143	14,30	2,20	30,23	Air213	15,43	3,65	49,98

4 DISCUSSION

Welding experiments without the root side shielding were also conducted to compare the argon and helium root side purging effects.

Increasing the arc welding time from 7 s to 21 s, as expected, increased the volume of melted base metal in all experiments. The impact of arc time on fusion zone penetration and width, according to Tab. 6 is shown in Fig. 5.

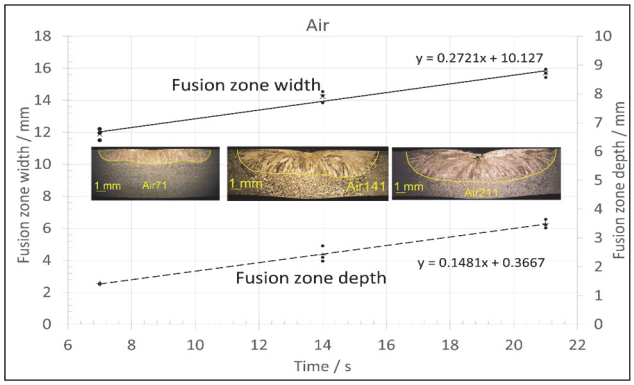

Figure 5 Characteristic values of fusion zone width and depth of unpurged or unprotected weld root side in contact with stagnant air

Mean *FZ* widths evolved from the lowest value of 11,88 mm (7 s) over 14,23 mm (14 s) to a maximum 15,69 mm for 21 s arc time.The average growth rate of fusion zone width (*FZW*) was relatively low (0,272 mm/s). The linear relation between *FZW* and welding time (*WT*) for unprotected weld root is expressed as:

$$FZW = 0{,}2721\ WT + 10{,}127 \quad (1)$$

The average *FZ* penetration growth rate was 0,148 mm/s. The mean fusion depth of 1,41 mm for 7 s welding time increased to 3,49 mm after 21 s. Linear relation between fusion zone depth (*FZD*) and welding time for unprotected weld root of 5 mm thick 316 ASS is described by the equation:

$$FZD = 0{,}1481\ WT + 0{,}3667 \quad (2)$$

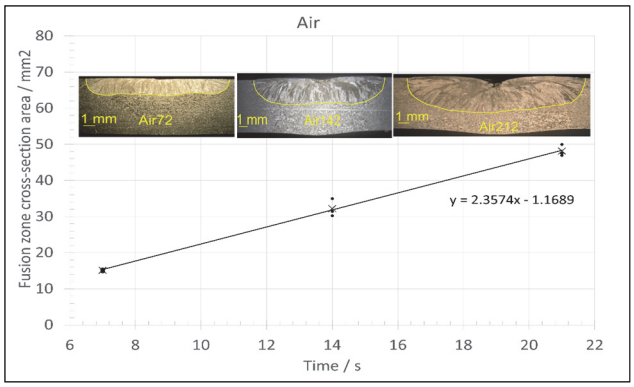

Figure 6 Weld cross-sectional area for unpurged weld root side for 7 s, 14 s and 21 s welding time

Three macrographs lined from left to right in Fig. 6 schematically show the average melted area of 15,14 mm^2 32,22 mm^2 and 48,14 mm^2 for 7 s, 14 s and 21 s welding time. The fusion zone area (*FZA*) also exhibited linear dependence with observed welding time.

$$FZA = 2{,}3574\ WT - 1{,}1689 \quad (3)$$

Weld cross-section area grew linearly and the average rate of growth was 2,357 mm^2/s for specimens welded with unpurged root side.

The measured welding thermal cycle for the welding time of 14 s and unprotected weld root side is presented in Fig. 7. The peak temperature reached 1262 °C.

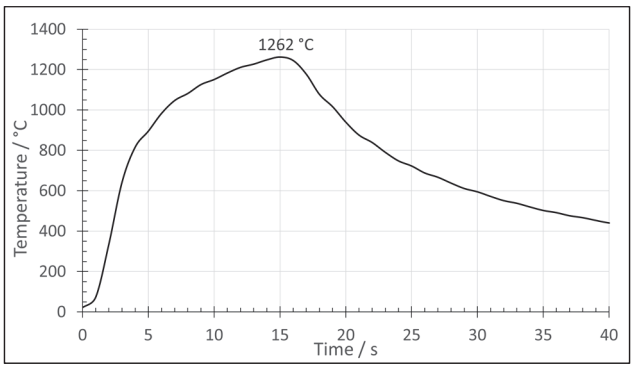

Figure 7 Thermal cycle for the specimen welded for 14 s with unpurged root side

The photographs in Fig. 8 show the unprotected weld root side for three investigated welding times (7 s, 14 s, 21 s) and the evolution of intense coloured oxides. The resulting colour is closely related to the thermal history of the root surface. The coloured area grew from the middle of the specimen's root side, exactly on the opposite side of the applied electric arc.

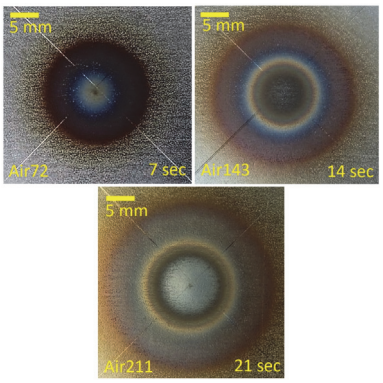

Figure 8 The evolution of the oxidised zone on the unprotected weld root side - outer diameter of optically noticeable brown area 19,45 mm, 27,37 mm and 32,77 mm for 7 s, 14 s and 21 s respectively

The introduction of argon as the protection of the weld root side resulted in a very similar linear dependency of *FZW* as in the case of unpurged welded specimens, Fig. 9.

Average *FZD* when purging the weld root side with Ar was 1,46 mm for 7 s arc time, 2,99 mm for 14 s and 3,90 mm for the longest tested welding time. The *FZD* growth rate of 0,174 mm/s was calculated and the linear relation to welding time in Arprotected weld root for 5 mm thick 316 ASS is described by the equation:

$$FZD = 0{,}174\ WT + 0{,}3489 \quad (4)$$

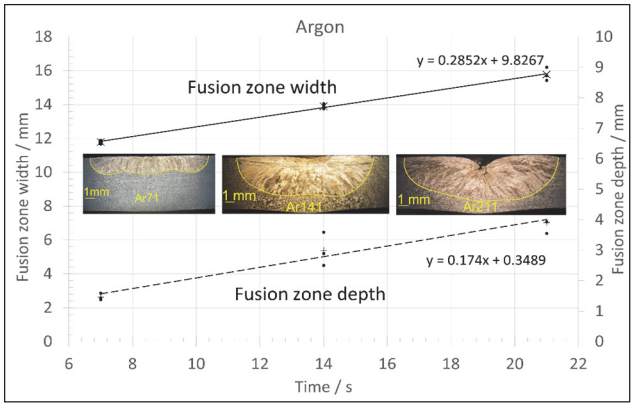

Figure 9 Weld penetration depth and width obtained in experiments with argon as the purging gas (10 l/min) for 7 s, 14 s and 21 s welding time

Fig. 10 also reveals a linear correlation between the fusion zone area (*FZA*) and welding time:

$$FZA = 2{,}593\ WT - 0{,}8067 \quad (5)$$

Selected macrographs in Fig. 10 represent mean fusion zone cross-section area of 14,70 mm^2(7 s), 35,35 mm^2(14 s) and 45,68 mm^2(21 s) for different welding time.

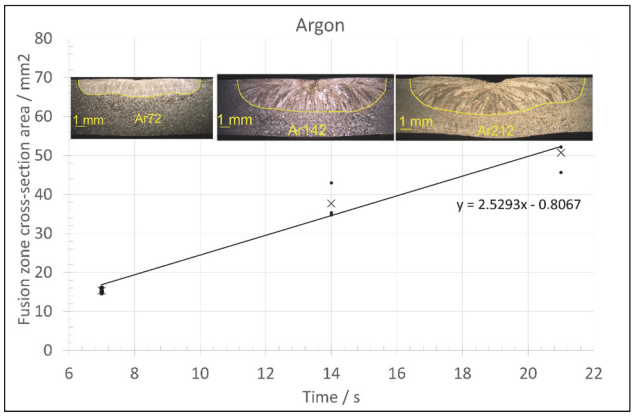

Figure 10 Weld cross-sectional area for application of argon as the purging gas (10 l/min) for 7 s, 14 s and 21 s welding time

Using helium as a weld root side purging gas revealed linear dependency between *FZW* and welding time. The *FZW* growth rate was slightly higher compared to the unprotected welded specimens and those purged by argon, Fig. 11. On the other hand, it is clear that penetration depth is lower when helium root side purging was used.

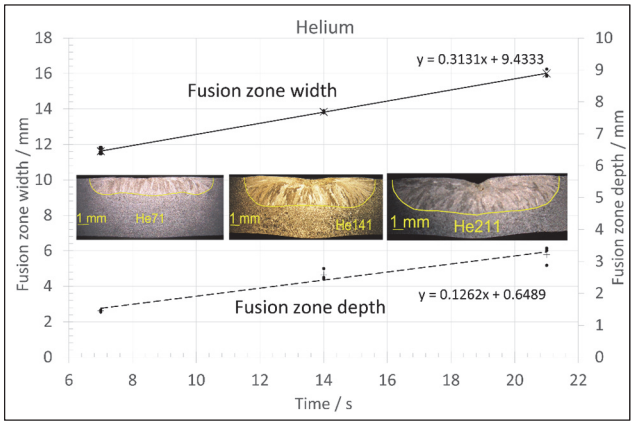

Figure 11 Weld penetration depth and width obtained in experiments with helium as the purging gas (4 l/min) for 7 s, 14 s and 21 s welding time

Fig. 12 reveals a linear relationship between the fusion zone area (*FZA*) and welding time when helium was applied as root side purging gas:

$$FZA = 2{,}0114\ WT + 2{,}7333 \quad (6)$$

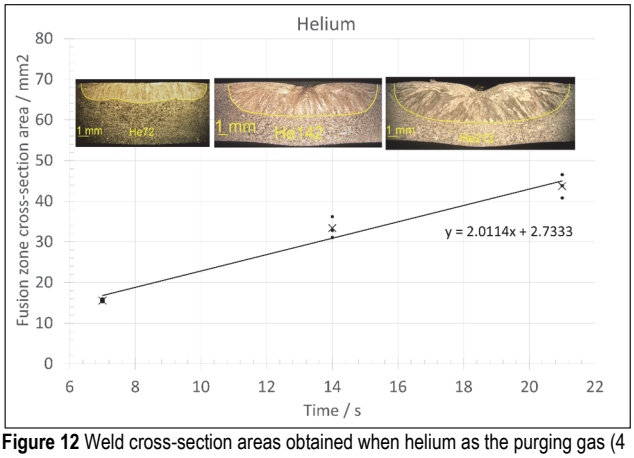

Figure 12 Weld cross-section areas obtained when helium as the purging gas (4 l/min) protected root side for 7 s, 14 s and 21 s welding time

Measured thermal cycles for argon and helium root side shielding and welding time of 14 seconds are shown in Fig. 13. The difference in peak temperature values is almost 100 °C as can be noticed in the graph.

The application of helium as a purging gas resulted in the lowest peak temperature compared with the other two welding conditions argon protected root side and root side exposed to the stagnant air.

This phenomenon can be explained by the excellent insulating characteristics (very low thermal conduction coefficient) of argon gas which decreased the specimen's root side cooling.

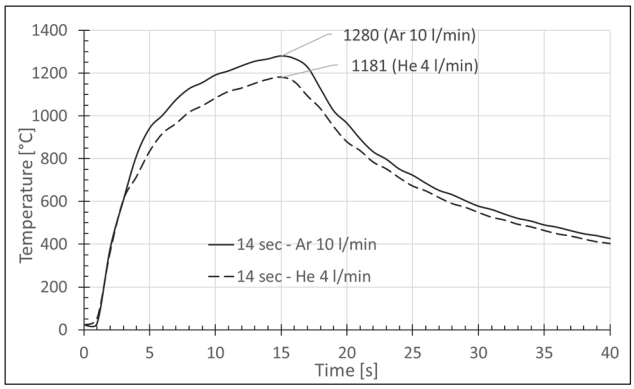

Figure 13 Thermal cycles for welding time 14 seconds and two different purging conditions on the weld root side

The measured thermal cycles for argon and helium weld root side shielding are compared with the thermal cycle for welding without root side shielding gas exposed to atmospheric air. The specimen's root side was cooled primarily by natural convection and the peak temperature value (1262 °C) was similar to the case when argon was used as root shielding gas.

Application of inert gases for the protection of weld root side ensured the absence of oxide film thickening, Fig. 14. Slight yellow straw colour can be seen but according to the recommendations it is the allowed condition.

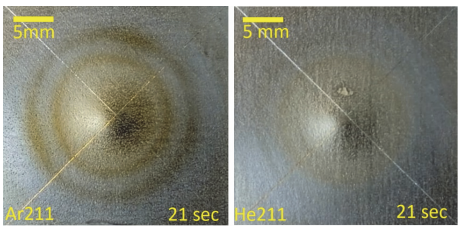

Figure 14 Weld root side surfaces after welding for 21 seconds purged with Ar (left) and helium (right)

Weld fusion zone width evolved almost identically throughout welding times from 7 s to 21 s regardless of whether the unpurged or purged condition (He or Ar) was applied on the 316L root side. All FZ widths were between 11,5 mm (minimum, Tab. 6) and 12,2 mm (maximum, Tab. 7). Experimental data are summarised in Fig. 15. Very similar growth rates of *FZ* width are calculated for argon (0,29 mm/s), helium (0,31 mm/s) and air (0,27 mm/s). The variability of measured width within every category is relatively small, the maximum range of 0,7 mm is found for specimens whose root side was unprotected, which is still below 6% of the calculated mean value.

FZ penetration depth evolution revealed linear dependency with welding time in three scenarios unprotected root side, He purged and Ar purged root side, Fig. 16. However, the penetration depth increased faster in the case of argon root side shielding (0,174 mm/s) compared to helium (0,126 mm/s) and air (0,148 mm/s).

The obvious difference in resulting fusion zone depth (penetration) between specimens whose root side was purged using argon or helium gas is shown in Fig. 17.

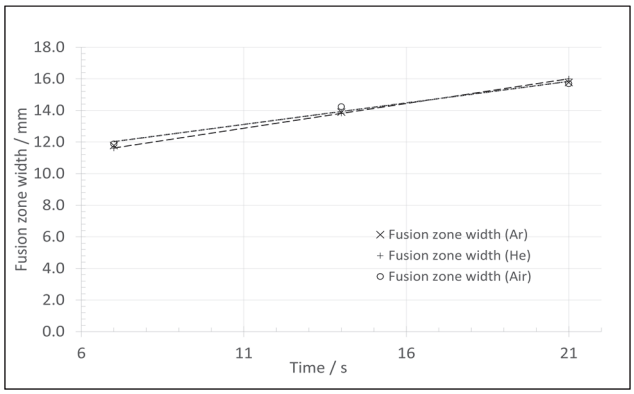

Figure 15 Time evolution of weld fusion zone width for purged (Ar and He) and unpurged conditions and 7 s, 14 s and 21 s

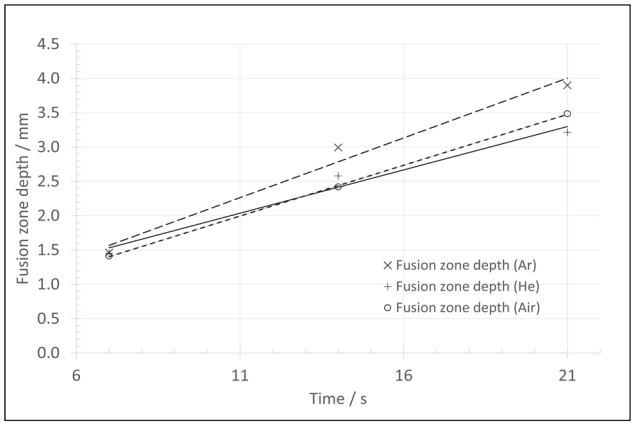

Figure 16 Comparison of weld penetration depth evolution for purged (Ar and He) and unpurged condition and arc welding times between 7s and 21 s

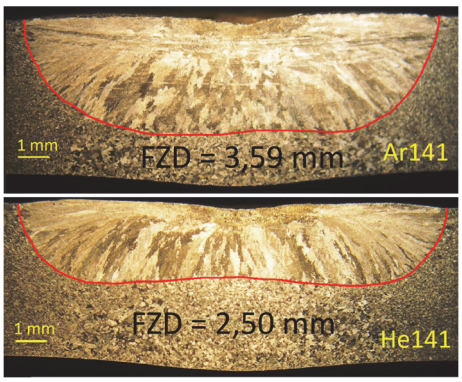

Figure 17 Penetration profiles and fusion zone depths for argon and helium weld root side shielding (welding time 14s)

The evolution of the fusion zone cross-section area for three different protection scenarios on the weld root side during welding from 7 to 21 seconds is shown in Fig. 18. The calculated growth of the fusion zone cross-section area for argon, helium and air on the weld root side were 2,53 mm^2/s, 2,01 mm^2/s and 2,36 mm^2/s respectively. The application of argon as a purging gas resulted in the fastest *FZ* area growth rate.

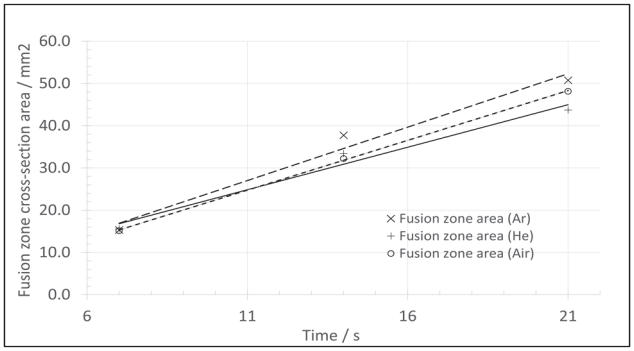

Figure 18 Time evolution of weld fusion zone cross-section area for purged (Ar and He) and unpurged condition (Air) and 7 s, 14 s and 21 s arc time

An example of weld fusion zone evolution in stationary autogenous TIG welding of 5 mm thick 316L stainless steel up to 21 s of welding time and argon purging gas is represented schematically in Fig. 19.

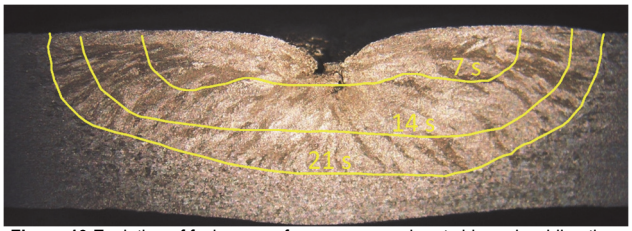

Figure 19 Evolution of fusion zone for argon purged root side and welding time 7 s, 14 s and 21 s

The weld root side argon purging resulted in the greatest *D*/*W* ratio, as shown in Fig. 20. This is expected because fusion zone width remained approximately similar for three cases but fusion zone depth increased if argon root side shielding was applied.

The rate of growth for the average fusion zone depth-to-width (*D*/*W*) ratio for argon was 0,009 mm/mm s which is almost double compared to helium (0,005 mm/mm s).

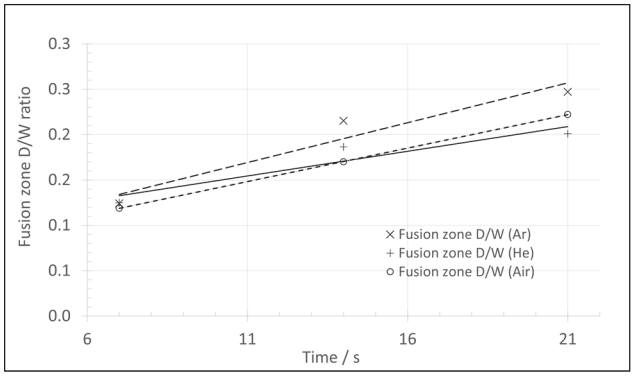

Figure 20 D/W ratio for purged (Ar and He) and unpurged condition (Air) for 7 s, 14 s and 21 s arc time

This result may be explained by the significant difference in thermal properties between used purging gases and air. In particular, the thermal conductivity of argon, helium and air are $26 \cdot 10^{-3}$ W/mK, $225 \cdot 10^{-3}$ W/mK and $41 \cdot 10^{-3}$ W/mK (data at 500 K), [26]. Although heat transfer from a heated root side can be influenced by convection in the presented experimental setup it is to be assumed that the thermal conductivity of the applied gases dominated heat transfer intensity. Therefore, argon's insulating property increased penetration depths for 14 s and 21 s welding time. For shorter welding time (7 s) all three penetration depths were almost identical (1,46 mm Ar, 1,45 He mm and 1,41 mm for air).

The fusion zone shape generally was axisymmetric and for shorter welding time was rather shallow and flat (low *D*/*W* ratio), Fig. 21. Prolonged welding time somewhat changed the fusion zone profile by increasing central penetration and resulting in a more conventional fusion zone shape.

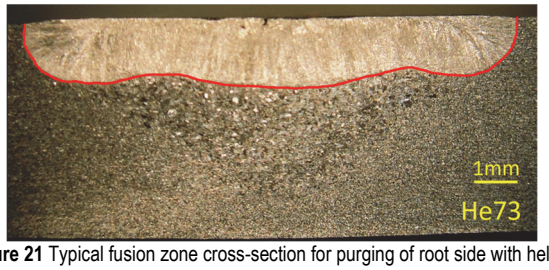

Figure 21 Typical fusion zone cross-section for purging of root side with helium and welding time of 7 seconds

5 CONCLUSIONS

The main goal of the present study was to investigate the influence of purging gas type on the fusion zone for the autogenous stationary TIG welding of austenitic stainless steel 316L.

The weld root side purging with argon (gas flow 10 l/min) and helium (4 l/min) under the selected welding parameters (150 A DC, EN, 45º vertex angle of 2% Th W electrode with no truncation, electrode tip to BM gap 3 mm, ESO 3 mm, Ar 8 l/min) for welding time of 7 s, 14 s and 21 s resulted in the following conclusions:

- No significant influence of the weld root side gas type on fusion zone width was observed.
- Fusion zone width time evolution was linear regardless of gas type on the weld root side.
- Compared to unprotected weld root side and helium purging, the presence of argon on the root side increases the fusion zone depth. For 14 seconds of welding time, penetration depth was on average 16% higher for argon than for helium. That difference was even higher (21%) for 21 s welding time. This beneficial effect of argon root purging can be attributed to its low thermal conductivity and possibly can be used in welding practice.
- When argon purging was applied, higher peak temperatures on the weld root surface were measured than in the case of helium purging. This observation is in accordance with increased fusion zone depth for argon root shielding.
- The shape of the weld fusion zone was approximately axisymmetric. For shorter welding time it was shallow and flat (low *D*/*W* ratio) but it resulted in a more conventional fusion zone shape for longer welding time when central penetration increased.
- The most sensitive variable of *FZ* characteristic features was penetration depth. Its variability was lower for shorter arc time (approximately 2%) and reached the value of 13 % for prolonged arc times.
- Application of both purging gases under chosen flow rates prevented severe oxidation and ensured the acceptable quality of weld root side surfaces.

6 REFERENCES

[1] Lippold, J. C. & Kotecki, D. J. (2005). *Welding Metallurgy and Weldability of Stainless Steel*. Hoboken: John Wiley & Sons.

[2] Folkhard, E. (1988). *Welding Metallurgy of Stainless Steels*. Vienna: Springer Vienna. https://doi.org/10.1007/978-3-7091-8965-8

[3] American Welding Society (2004). *Welding Handbook: Welding Processes*, Part 1. Miami: American Welding Society.

[4] Aucott, L., Dong, H., Mirihanage, W., Atwood, R., & Kidess, A. et al. (2018). Revealing internal flow behaviour in arc welding and additive manufacturing of metals. *Nature Communications*, *9*(1), 1-7. https://doi.org/10.1038/s41467-018-07900-9

[5] DebRoy, T. & David, S. A. (1995). Physical processes in fusion welding. *Reviews of Modern Physics*, *67*(1), 85-112. https://doi.org/10.1103/RevModPhys.67.85

[6] Wu, F., Falch, K. V., Guo, D., English, P., Drakopoulos, M., & Mirihanage, W. (2020). Time evolved force domination in arc weld pools. *Materials & Design*, 1901-1908. https://doi.org/10.1016/j.matdes.2020.108534

[7] Huang, H., Shyu, S., Tseng, K., & Chou, C. (2006). Efects of the Process Parameters on Austenitic Stainless Steel by TIG-Flux Welding. *Journal of Materials Science & Technology*, *22*(3), 367-374.

[8] Huang, H. Y. (2009). Effects of shielding gas composition and activating flux on GTAW weldments. *Materials and Design*, *30*(7), 2404-2409. https://doi.org/10.1016/j.matdes.2008.10.024

[9] Shirali, A. & Mills, K. (1993). The effect of welding parameters on penetration in GTA welds. *Welding journal*, *72*(7), 347-353.

[10] Jamshidi Aval, H., Farzadi, A., Serajzadeh, S., & Kokabi, A. H. (2009). Theoretical and experimental study of microstructures and weld pool geometry during GTAW of 304 stainless steel. *International Journal of Advanced Manufacturing Technology*, *42*(11-12), 1043-1051. https://doi.org/10.1007/s00170-008-1663-6

[11] Lu, S. P., Fujii, H., Nogi, K., & Sato, T. (2007). Effect of oxygen content in He-O2 shielding gas on weld shape in ultra deep penetration TIG. *Science and Technology of Welding*

and Joining, *12*(8), 689-695. https://doi.org/10.1179/174329307X238425
[12] Durgutlu, A. (2004). Experimental investigation of the effect of hydrogen in argon as a shielding gas on TIG welding of austenitic stainless steel. *Materials and Design*, *25*(1), 19-23. https://doi.org/10.1016/j.matdes.2003.07.004
[13] Burgardt, P. & Heiple, C. R. (1986). Interaction between Impurities and Welding Variables in Determining GTA Weld Shape. *Welding Journal*, *2*(6), 150-155.
[14] Heiple, C. R. & Roper, J. R. (1982). Mechanism for Minor Element Effect on GTA Fusion Zone Geometry. *Welding Journal*, *61*(4), 97-102.
[15] Giridharan, P. K. & Murugan, N. (2009). Optimization of pulsed GTA welding process parameters for the welding of AISI 304L stainless steel sheets. *International Journal of Advanced Manufacturing Technology*, *40*(5-6), 478-489. https://doi.org/10.1007/s00170-008-1373-0
[16] Lothongkum, G., Viyanit, E., & Bhandhubanyong, P. (2001). Study on the effects of pulsed TIG welding parameters on delta-ferrite content, shape factor and bead quality in orbital welding of AISI 316L stainless steel plate. *Journal of Materials Processing Technology*, *110*(2), 233-238. https://doi.org/10.1016/S0924-0136(00)00875-X
[17] Pandya, D., Badgujar, A., & Ghetiya, N. (2021). A novel perception toward welding of stainless steel by activated TIG welding: a review. *Materials and Manufacturing Processes*, *36*(8), 877-903. https://doi.org/10.1080/10426914.2020.1854467
[18] Tathgir, S., Bhattacharya, A., & Bera, T. K. (2015). Influence of current and shielding gas in TiO2 flux activated TIG welding on different graded steels. *Materials and Manufacturing Processes*, *30*(9), 1115-1123. https://doi.org/10.1080/10426914.2014.973591
[19] Qi, B. J., Yang, M. X., Cong, B. Q., & Liu, F. J. (2013). The effect of arc behavior on weld geometry by high-frequency pulse GTAW process with 0Cr18Ni9Ti stainless steel. *International Journal of Advanced Manufacturing Technology*, *66*(9-12), 1545-1553. https://doi.org/10.1007/s00170-012-4438-z
[20] Feng, Y., Luo, Z., Liu, Z., Li, Y., Luo, Y., & Huang, Y. (2015). Keyhole gas tungsten arc welding of AISI 316L stainless steel. *Materials and Design*, 8524-31. https://doi.org/10.1016/j.matdes.2015.07.011
[21] Stadler, M., Freton, P., & Gonzalez, J. J. (2017). Influence of Welding Parameters on the Weld Pool Dimensions and Shape in a TIG Configuration. *Applied Sciences*, *7*(4), 373. https://doi.org/10.3390/app7040373
[22] Taban, E., Kaluc, E., & Aykan, T. S. (2014). Effect of the purging gas on properties of 304H GTA welds. *Welding Journal*, *93*(4),
[23] Westin, E. M., Johansson, M. M., & Pettersson, R. F. A. (2013). Effect of nitrogen-containing shielding and backing gas on the pitting corrosion resistance of welded lean duplex stainless steel LDX 2101® (EN 1.4162, UNS S32101). *Welding in the World*, *57*(4), 467-476. https://doi.org/10.1007/s40194-013-0046-2
[24] Panmongkol, P. & Phung-on, I. (2021). Effect of backing gas mixtures on corrosion properties of stainless steel grade 304 weld metal by autogenous GTAW. *Journal of Materials Research and Technology*, 111559-111570. https://doi.org/10.1016/j.jmrt.2021.01.125
[25] Pichler, P., Simonds, B. J., Sowards, J. W., & Pottlacher, G. (2020). Measurements of thermophysical properties of solid and liquid NIST SRM 316L stainless steel. *Journal of Materials Science*, *55*(9), 4081-4093. https://doi.org/10.1007/s10853-019-04261-6
[26] Boulos, M. I., Fauchais, P., & Pfender, E. (1994). Thermal Plasmas - Fundamentals and Applications, 1. https://doi.org/10.1007/978-1-4899-1337-1_1

Contact information:

Domagoj KOJUNDŽIĆ, Mag. Ing. Mech. Eng., PhD Student
(Corresponding author)
Faculty of Electrical Engineering,
Mechanical Engineering and Naval Architecture,
Ruđera Boškovića 32, 21000 Split, Croatia
E-mail: dkojundz@fesb.hr

Nikša KRNIĆ, Associate Professor, PhD.
Faculty of Electrical Engineering,
Mechanical Engineering and Naval Architecture,
Ruđera Boškovića 32, 21000 Split, Croatia
E-mail: nkrnic@fesb.hr

Ivan SAMARDŽIĆ, Full professor tenure, PhD.
University of Slavonski Brod, Mechanical Engineering Faculty in Slavonski Brod,
Trg Ivane Brlić Mažuranić 2, 35000 Slavonski Brod, Croatia
E-mail: ivan.samardzic@unisb.hr

Pejo KONJATIĆ, Associate Professor, Ph. D.
University of Slavonski Brod, Mechanical Engineering Faculty in Slavonski Brod,
Trg Ivane Brlić Mažuranić 2, 35000 Slavonski Brod, Croatia
E-mail: pejo.konjatic@unisb.hr